



Cite this: *Analyst*, 2022, **147**, 4426

Serum fingerprinting by slippery liquid-infused porous SERS for non-invasive lung cancer detection†

Chenlei Cai,^{‡a} Yujie Liu,^{‡b} Jiayu Li,^a Lei Wang^{*a} and Kun Zhang ^{*b}

Lung cancer (LC) remains the most commonly diagnosed cancer. Timely diagnosis is crucial for improving the clinical outcomes of LC patients. Serum molecular patterns reflect the physiological and pathological status of individuals, and are promising as diagnostic targets for malignancies. Here, we report a spectroscopic method for the rapid identification of LC based on the label-free fingerprinting of clinical serum samples with slippery liquid-infused porous surface-enhanced Raman spectroscopy (SLIPSERS). We first demonstrate the capability of SLIPSERS for the delivery and preconcentration of serum molecules into the SERS hot spots from an evaporating liquid droplet, enabling the acquisition of vibrational fingerprints of serum molecules with only 1 μL of blood serum in minutes. The averaged SLIPSERS signals of the serum sample from a cohort of 33 LC patients and 23 healthy controls reveal both metabolic and biomacromolecular alterations under LC conditions. By analyzing the SLIPSERS data with chemometric methods, we further demonstrate that the SLIPSERS profiling of serum molecular patterns allows the reliable discrimination of LCs from healthy controls. Considering the ease of operation and high efficiency, our SLIPSERS-based serum biopsy method should hold great potential for non-invasive LC diagnosis.

Received 12th August 2022,
Accepted 8th September 2022

DOI: 10.1039/d2an01325h

rsc.li/analyst

Introduction

Lung cancer (LC) is the leading cause of cancer mortality worldwide, with an estimated 1.8 million deaths each year.¹ Despite the availability of new treatments, about 75% of LC cases are diagnosed at the advanced stages where treatments are less effective, ultimately leading to poor prognosis and a low 5-year survival rate of <20%.^{2–5} Early diagnosis is crucial to improve the clinical outcomes of patients.⁶ Low-dose computed tomography (LDCT) screening has led to a significant decrease in LC mortality among high-risk persons.^{7,8} However, LDCT has some disadvantages, including the high false-positive rate, overdiagnosis, and radiation exposure, which can limit its application in the longitudinal monitoring of disease and therapeutic response.⁹ Hence, there is an unmet need to develop alternative non-invasive approaches to LC diagnosis.

Molecular biopsy in blood offers an attractive means of managing LC by analysing circulating tumour biomarkers in a less invasive and repeatable way.^{10–12} The targeted detection of blood proteins and nucleic acids has been attempted and found to be useful in LC evaluation.^{12–15} For example, the quantification of exosomal PD-L1 in the blood allows LCs to be distinguished from healthy controls and tracking of the response to immunotherapy.¹⁶ Despite their utility, biomarker-based targeted assays often suffer from tedious manipulations such as sample isolation, labelling, amplification, and multiple washings, insufficient specificity to tumour heterogeneity, and more importantly, the risk of failing to capture unknown, potentially diagnostic markers. In this regard, direct label-free profiling of the blood serum/plasma can provide a simpler and more efficient access to the tumour molecular profile.^{17–25}

Raman spectroscopy allows the extraction of molecular fingerprints by measuring the inelastic scattering spectra associated with molecular vibration and rotation.²⁶ Although the Raman response of biomolecules is weak, surface-enhanced Raman spectroscopy (SERS) can largely enhance the signal intensity *via* excitation of the localized surface plasmon resonance of metal nanostructures, thus enabling sensitive chemical and biological analysis.^{27,28} As a non-destructive analytical technique, SERS has been successfully used for direct profiling of the molecular patterns from extracellular vesicles, live cells, biofluids, and even tissues.^{29–34} Han *et al.* reported that the

^aDepartment of Medical Oncology, Shanghai Pulmonary Hospital, Tongji University School of Medicine, Shanghai, 200433, China. E-mail: wangleixxxn@163.com

^bShanghai Institute for Pediatric Research, Shanghai Key Laboratory of Pediatric Gastroenterology and Nutrition, Xinhua Hospital, Shanghai Jiao Tong University School of Medicine, Shanghai 200092, China. E-mail: kunzhang@shsmu.edu.cn

†Electronic supplementary information (ESI) available. See DOI: <https://doi.org/10.1039/d2an01325h>

‡These authors contributed equally to this work.

SERS profiling of plasma-derived exosomes could be used for the detection of osteosarcoma.²⁹ Few studies have proved the feasibility of direct SERS fingerprinting of patient serum for LC diagnosis.^{35,36} Notably, a prerequisite for obtaining high-quality Raman spectra of biomolecules is to place them in SERS-active regions (the so-called electromagnetic hotspots). The evaporation of an aqueous droplet containing analytes on a plasmonic substrate is one of the most common approaches used to acquire SERS fingerprints of a sample.²⁷ Unfortunately, diffusion of molecules over the hydrophilic substrate during evaporation can result in insufficient molecular adsorption in the SERS-sensitive regions, and thereby SERS signatures with a low signal-to-noise ratio and reproducibility. The deployment of superhydrophobic surfaces provides an effective way for enriching analytes at the plasmon-active region, and hence improving the quality of SERS spectra.^{29,33} The rapid fabrication of superhydrophobic SERS substrates, however, remains an experimental challenge. The current methods require either precise micro/nano engineering or time-cost surface fluorosilylation, which hampers rapid and large-scale clinical testing. Slippery liquid infused porous SERS (SLIPSERS) is a simple yet effective method for the manipulation and SERS detection of analytes on the basis of droplet evaporation on a slippery, omniphobic surface.³⁷ By biomimicking the natural pitcher plant, SLIPS provides a nearly pinning-free substrate, enabling the simultaneous complete enrichment of analytes and SERS matrices (*e.g.*, gold nanoparticles (Au NPs)) within an evaporating liquid droplet. The accumulation of analytes at the tiny detection area gives rise to a largely amplified SERS signal.^{37–41} Although highly feasible for the measurement of trace molecules in standard solutions, the SLIPSERS technique has not yet been adapted for extracting cancer-associated molecular patterns from clinical serum samples.

Here we report the first SLIPSERS analysis of a patient serum (1 μL) for LC diagnosis (Fig. 1). The use of the slippery substrate enables serum components to be enriched and delivered into the SERS-active area, without external optical, electrical, magnetic, and thermal forces. We show that the rich electromagnetic hotspots and high local concentration of serum components in SLIPSERS permit high-fidelity acquisition of serum Raman fingerprints with abundant tumour-specific molecular information. The multivariate analysis of SLIPSERS spectra allows the identification of LC from healthy controls. Our results reveal that label-free serum analysis by

SLIPSERS has great potential for the non-invasive diagnosis of LC.

Experimental section

Chemicals

Au NPs (1 OD, 60 nm) were purchased from BBI solutions (Cardiff, UK), which were characterized by UV-vis spectroscopy (Nanodrop 2000) and transmission electron microscopy (TEM, JEOL JEM-2100F) (Fig. S1 and S2[†]). Teflon membranes (200 nm pore size, 75 μm thickness) were purchased from ADVANTEC (Tokyo, Japan). The DuPont Krytox perfluoropolyether GPL 103 lubricant was purchased from the Chemours Company. Deionized water (resistivity 18.2 $\text{M}\Omega\text{ cm}$) purified on a MilliQ (Millipore, Germany) system was used for the preparation of all aqueous solutions.

Slippery substrate preparation

Teflon membranes (diameter 3 mm) were attached on a glass slide with double-sided adhesive tape. Dupont GPL 103 was then pipetted onto the Teflon membranes. The lubricated membranes were then spun at 3000g for 10 s to remove the excess lubricating liquid.

Serum preparation

Blood samples in red-topped vacuum blood collection tubes with a clot activator were kept upright for 0.5–1 h at room temperature. After clotting, the samples were centrifuged at 2000g for 10 min at 4 $^{\circ}\text{C}$. The serum in the supernatant was collected and ultrafiltered through a 3 kDa ultrafiltration tube (Sartorius). The deproteinized serum was aliquoted and stored at $-80\text{ }^{\circ}\text{C}$ for further use. This study was approved by the ethics committee of Shanghai Pulmonary Hospital affiliated to Tongji University (L20-337-1). A written informed consent was obtained from each participant.

SLIPSERS detection

First, Au NPs were concentrated tenfold (10 OD) by centrifugation at 4500 rpm for 5 min. 5 μL of Au NPs was fully mixed with 1 μL of serum, and then loaded onto the slippery membrane substrate with a pipette. The sample was kept at 60 $^{\circ}\text{C}$ to evaporate the solvent and form a small black aggregate, which consisted of closely packed Au NPs and the serum components. SERS fingerprinting was conducted on this aggregate

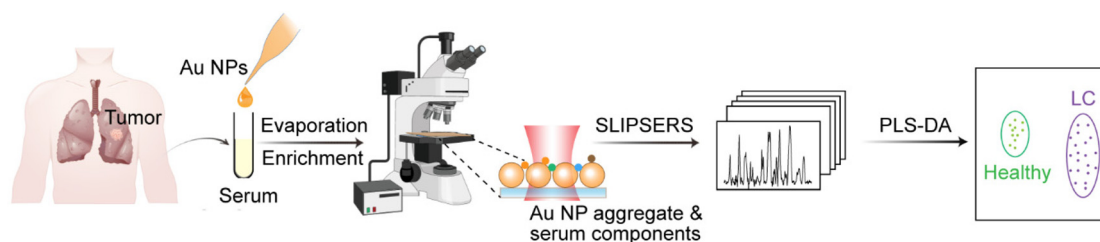


Fig. 1 Schematic illustration of SLIPSERS fingerprinting of blood serum for the identification of lung cancer.

using a home-built upright confocal Raman microscope equipped with a 638 nm He–Ne laser, a 50× (NA = 0.55) objective lens, and an Andor SR500i-D2 spectrometer with a 600 grooves per mm grating. The SERS spectra were recorded in the range of 400–1800 cm^{-1} . At least five different spectra were collected from each substrate and three replicates for individual serum samples were recorded. The laser power on the sample surface was 0.5 mW. The acquisition time for each spectrum was 0.5 s with 20 accumulations. Prior to determination, the system was calibrated with the Raman peak of single crystalline silicon at 520.7 cm^{-1} .

Analysis of SLIPSERS data

Before analysis, the raw SLIPSERS spectra were subjected to the following pre-treatments: (a) removing the cosmic rays; (b) smoothing with the Savitzky–Golay filter (polynomial order 3 and points of window 11); and (c) baseline correction with the asymmetric least-squares method. Multivariate statistical analysis including principal component analysis (PCA), partial least squares discriminant analysis (PLS-DA), orthogonal projections to latent structures-discriminant analysis (OPLS-DA), and receiver operating characteristic (ROC) curve analysis (Tester) were performed using MetaboAnalyst 5.0 (McGill University, Montreal, Canada, <https://www.metaboanalyst.ca/>).

Results and discussion

Characterization of SLIPSERS

The slippery substrate was prepared by spin coating of the perfluorinated lubricant (DuPont Krytox GPL 103) on a Teflon membrane (200 nm pore size) (see details in the Experimental section). As previously observed by Wong and others,^{37–41} the low surface tension enables the perfluorinated substrate to be immiscible for aqueous solutions, providing a quite simple yet effective means for the delivery and enrichment of analyte molecules within the SERS hotspots by pinning-free droplet evaporation (Fig. 2a). To demonstrate this, we first pipetted 5 μL of Au NP solution (10 OD) containing 10^{-10} mole of methylene blue onto the slippery substrate, followed by standing for 5 min at 60 °C to allow for droplet evaporation. As demonstrated in Fig. 2b, the evaporation of the mixture solution results in clustering of the metal NPs at the membrane surface to form a small bluish-black aggregate. We monitored changes in the droplet size during evaporation and observed a 1.53-fold decrease in the diameter of the liquid droplet after drying (Fig. 2c). No apparent Au particles and dye molecules were observed outside the NP aggregate, indicating a high collection efficiency of the SLIPS substrate (Fig. 2b and S3†). Scanning electron microscopic (SEM) analysis reveals that Au NPs are closely packed into a 3D multilayer architecture in the aggregate (Fig. 2d), forming a large number of densely distributed plasmonic hotspots for Raman enhancement, as theoretically supported by the numerical electromagnetic simulation (Fig. 2e). The SERS characterization further demonstrates that the Raman signal of methylene blue is only enhanced by the

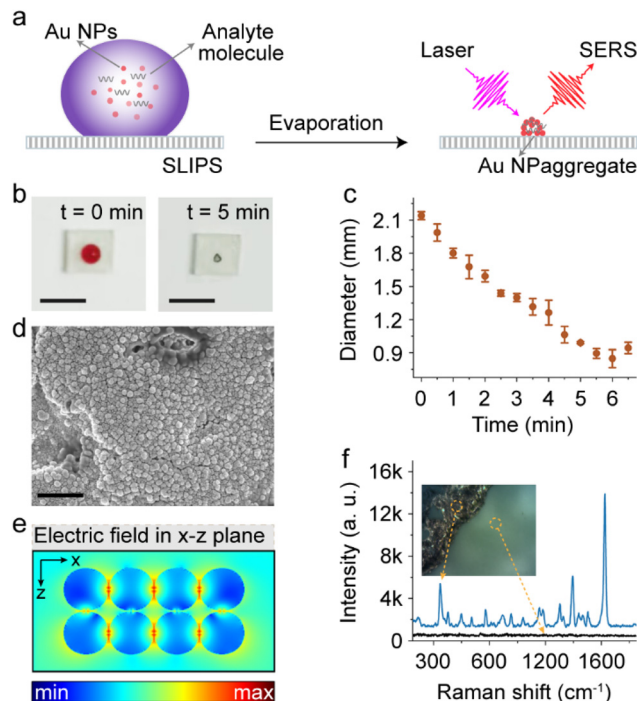


Fig. 2 SLIPS characterization. (a) Scheme of SLIPSERS detection. (b) Optical photographs of Au NPs before and after solvent evaporation on the SLIP surface. The brightness and contrast of the photographs were adjusted slightly for visualization. Scale bars: 5 mm. (c) Time-dependent variation of the droplet diameter during evaporation. (d) The SEM image of closely packed Au NPs in the 3D aggregate. Au spraying was conducted to improve the sample conductivity. Scale bar: 1 μm . (e) FDTD simulation showing spatial distribution of the electric field at Au surfaces upon 638 nm laser excitation. (f) SLIPSERS detection of methylene blue (10^{-10} mol) from the 3D Au aggregate and the bare SLIP surface. The spectra were vertically translated for clarity.

closely packed Au NPs (see peak assignments in Table S1†), with no SERS signal in the surrounding area. These results indicate that the SLIPSERS platform allows for the highly efficient concentration and detection of analytes in aqueous fluids.

SLIPSERS fingerprinting of the human serum

Having confirmed the ability of SLIPSERS with regard to the preconcentration and detection of analytes in liquid solutions, we investigated whether this platform could be applied to clinical serum samples. We collected the blood serum from 33 patients pathologically diagnosed with non-small-cell lung cancer and 23 healthy controls. 5 μL of Au NPs was mixed with 1 μL of deproteinized serum, and then subjected to SLIPSERS analysis. An intense SERS signal was observed from the Au NP aggregate compared to that of the PBS control (Fig. 3a). To minimize the effect of background signals, spectral preprocessing, including cosmic ray removal, denoising, baseline correction, and min–max normalization, was conducted before further data analysis (Fig. S4†). As shown in Fig. 3b, the normalized SERS signatures are reproducible across different sites of the serum containing the Au NP cluster, although a moder-

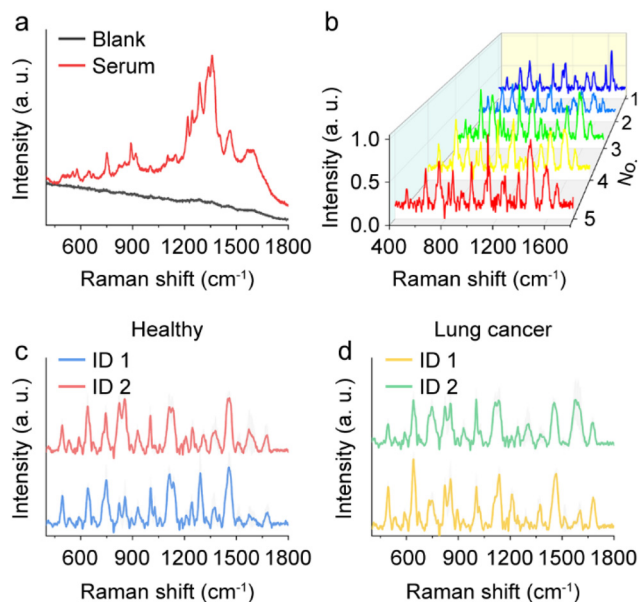


Fig. 3 (a) SLIPSERS spectra of Au NP–PBS and Au NP–serum mixtures. (b) SLIPSERS spectra of the serum collected from five different locations of the Au NP aggregate surface. (c) Mean SLIPSERS spectra of serum samples from two healthy controls. (d) Mean SLIPSERS spectra of serum samples from two lung cancer patients.

ate variation in the relative intensities of some peaks can be observed. The relative standard deviation (RSD) values of the major band intensities vary in the range from 7.66% to 33.9% with a median value of 18.57%. We infer that the variation is caused by the chemical complexity of the serum, and the fact that a few molecules located in the tiny hot spots contribute to most of the signal response in SERS.⁴² To this end, multiple spectra per sample were measured with three replicates for each serum. Fig. 3c shows the mean serum spectra of two healthy donors. The two spectra exhibit apparent differences between 750–900 cm^{-1} and 1100–1500 cm^{-1} , suggesting the

heterogeneity of the serum molecular pattern of individuals. Such spectral heterogeneity is also reflected by analysing the serum from LC patients (Fig. 3d).

Fig. 4a shows the SLIPSERS spectra of 33 LC patients and 23 healthy controls. Consistent with the above discussion, the signal heterogeneity between individual samples is very prominent. Nonetheless, we can observe some difference between the two groups. For example, the overall intensity of bands around 850 cm^{-1} in the LC group is slightly weaker than that in the healthy control group. In contrast, for peaks near 1600 cm^{-1} , the overall signal intensity in the patient group is somewhat greater than that in the healthy control group. To intuitively examine the spectral information for the two groups, the averaged SLIPSERS spectra of all LC patients and healthy controls are respectively plotted in Fig. 4b. As expected, the ensemble-averaged signals of the patient and control groups are quite similar, with abundant peaks arising from the metabolites, nucleic acids, and proteins (see the peak positions and assignments of the vibrational modes in Table S2, ESI[†]). The difference spectrum shows a signal increase in the range of 1550–1690 cm^{-1} (phenylalanine, amide I), and some degree of signal decrease at around 640 (tyrosine, lactose), 850 (tyrosine), 1050 (lipids, glycogen), and 1140 cm^{-1} (mannose) for the LC group. Our result is in accordance with the previous reports that many amino acids, saccharides, and lipids are downregulated in LC, while the levels of phenylamine and some proteins, such as histone H2A and thymopointin, are increased.^{43–45} It is worth noting that although we pretreated the serum samples by ultrafiltration, some small low-abundance proteins were retained, as evidenced by the BCA protein assay result (Fig. S5[†]).

SLIPSERS detection of NSCLC

Inspired by the above difference in the averaged serum SLIPSERS spectra, we performed multivariate statistical analysis to further inspect the utility of the serum SLIPSERS data in LC detection. The 56 serum samples were randomly

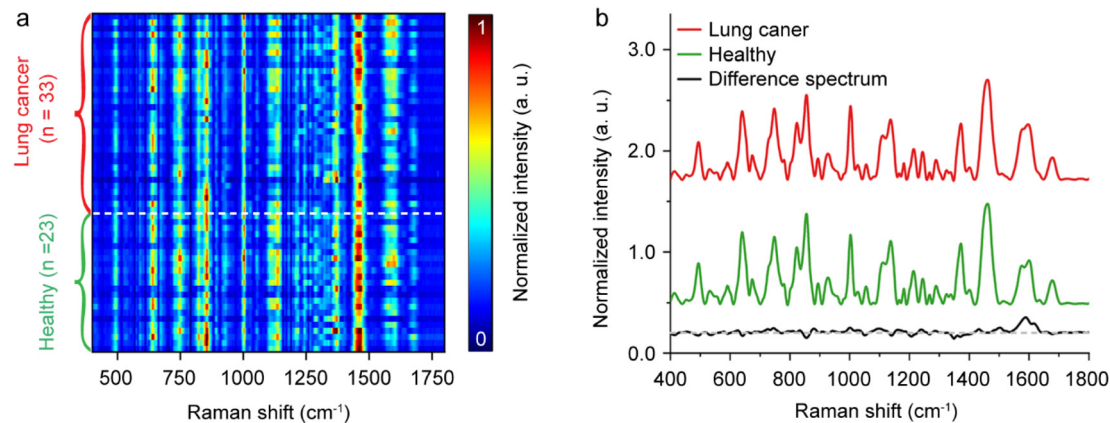


Fig. 4 (a) SERS spectra of lung cancer ($n = 33$) and healthy control groups ($n = 23$). (b) Mean SERS spectra of lung cancer ($n = 33$) and healthy control samples ($n = 23$) and their difference.

designated as a training dataset (23 patients and 13 controls) and a validation dataset (10 patients and 10 controls). Table S3† shows the baseline characteristics of the patients and controls. There is no significant difference in terms of age and gender among groups. We first attempted to analyse the 36 SLIPSERS spectra (the second derivative) of the training data with PCA. As shown in Fig. S6,† the SLIPSERS signals of serum samples from LC cases cannot be well differentiated from controls by PCA due to the high spectral similarity. PLS-DA was then utilized to analyse SLIPSERS fingerprints of the training data. PLS-DA is a supervised classification method, which combines dimensionality reduction and discriminant analysis into one algorithm and is especially applicable to modelling high dimensional data.⁴⁶ As shown in Fig. 5a, spectral data derived from the LC samples can be separated from those of the controls by PLS-DA (indicated by non-overlapping 95% confidence ellipses). In addition, discrimination of the spectral data was further challenged by performing OPLS-DA. In comparison with PLS-DA, OPLS-DA splits up the data variation into the variation related to the response and an orthogonal (noise) variation that is not related to the response, hence simplifying the interpretability of the obtained model and providing an estimation of within- and between-group variability.⁴⁷ Unsurprisingly, the spectral data between NSCLC cases and controls can also be differentiated by OPLS-DA as shown in Fig. 5b.

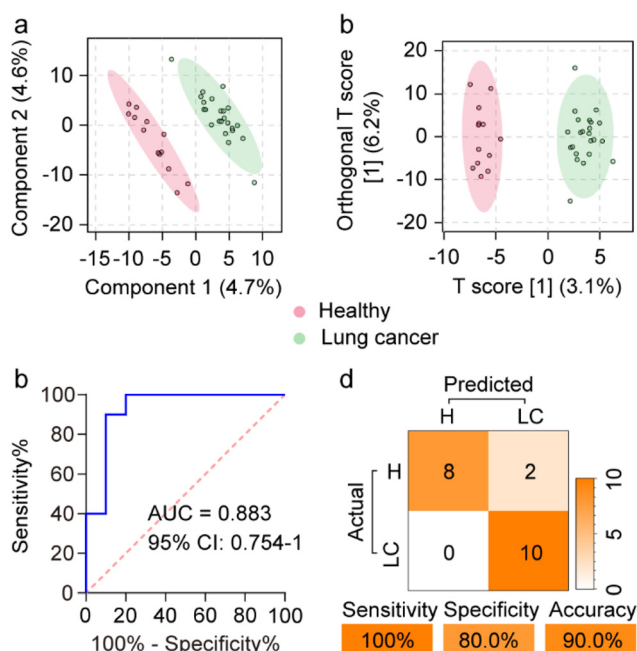


Fig. 5 PLS-DA (a) and OPLS-DA (b) score plots of SERS data of serum samples from 10 healthy controls and 20 lung cancer patients in the training dataset. (c) ROC analysis with cross-validation on the training dataset using the classification model built by PLS-DA. (d) Confusion matrix of the classification result of the validation dataset consisting of 10 healthy controls (H) and 10 lung cancer (LC) samples.

There are 98 and 110 features with variable importance for the projection (VIP) value >1.5 in PLS-DA and OPLS-DA, respectively. Fig. S7† shows the VIP values of the top 15 features. On the basis of these significant features, a diagnosis model was then built with PLS-DA integrated by Metaboanalyst for LC detection. The receiver operating characteristic (ROC) analysis of the training data yields a high area under the curve (AUC) value of 0.883 ($P = 0.0002$, sensitivity = 95.6%, specificity = 84.6%). When applying to the validation data, the model shows an AUC value of 0.930 ($P = 0.012$). The confusion matrix in Fig. 5d indicates that all LC samples were correctly identified and two control samples were misclassified as LC cases by the model in the validation set. The sensitivity, specificity, accuracy, and precision for LC detection are 100%, 80%, 90%, and 83.3% respectively. The result suggests that label-free molecular fingerprinting of the patient serum by SLIPSERS is a potentially promising method for the detection of LC.

Conclusions

In summary, we have demonstrated the direct fingerprinting of 1 μ L serum within minutes using SLIPSERS. We have shown that SLIPSERS is capable of the collection and precise delivery of analytes to dense SERS hotspots. The high local concentration of analytes and low spatial variability of plasmonic hotspots on SLIPSERS substrates illustrate the sensitivity and reproducibility of the approach. By combining multivariate statistical analysis with our SLIPSERS platform, we have demonstrated that it is possible to discriminate LC patients from healthy controls by the label-free spectral characterization of a clinical serum. Limitations of this work include the relatively small sample size. In addition, improvement of the spectral quality using engineered NPs such as core-shell or tip-enriched NPs needs further investigation. By designing advanced plasmonic NPs to analyse an expanded cohort of samples at different pathological stages, we believe that the SLIPSERS platform should shed light on the early non-invasive detection of LC at the molecular level.

Author contributions

Chenlei Cai: conceptualization, methodology, investigation, and writing – original draft. Yujie Liu: methodology, investigation and writing-original draft. Jiayu Li: investigation, writing – original draft, and funding acquisition. Lei Wang: conceptualization, supervision and writing – review & editing. Kun Zhang: conceptualization, methodology, writing – review & editing, supervision, and funding acquisition.

Conflicts of interest

There are no conflicts to declare.

Acknowledgements

This study was supported by the National Natural Science Foundation of China (nos 21974088 and 81902314), and the Shanghai Natural Science Foundation (no. 21ZR1481300). Fig. 1 was created using Figdraw (<https://www.figdraw.com>) and SciDraw (<https://scidraw.io>).

References

- H. Sung, J. Ferlay, R. L. Siegel, M. Laversanne, I. Soerjomataram, A. Jemal and F. Bray, *CA Cancer J. Clin.*, 2021, **71**, 209–249.
- Z. Chen, C. M. Fillmore, P. S. Hammerman, C. F. Kim and K.-K. Wong, *Nat. Rev. Cancer*, 2014, **14**, 535–546.
- M. M. Jacobsen, S. C. Silverstein, M. Quinn, L. B. Waterston, C. A. Thomas, J. C. Benneyan and P. K. J. Han, *Lung Cancer*, 2017, **112**, 156–164.
- C. Allemani, T. Matsuda, V. Di Carlo, R. Harewood, M. Matz, M. Nikšić, A. Bonaventure, M. Valkov, C. J. Johnson, J. Estève, O. J. Ogunbiyi, G. A. e Silva, W.-Q. Chen, S. Eser, G. Engholm, C. A. Stiller, A. Monnereau, R. R. Woods, O. Visser, G. H. Lim, J. Aitken, H. K. Weir, M. P. Coleman and CONCORD Working Group, *Lancet*, 2018, **391**, 1023–1075.
- F. Wu, L. Wang and C. Zhou, *Curr. Opin. Oncol.*, 2021, **33**, 40–46.
- N. Hawkes, *Br. Med. J.*, 2019, **364**, l408.
- H. J. de Koning, C. M. van der Aalst, P. A. de Jong, E. T. Scholten, K. Nackaerts, M. A. Heuvelmans, J.-W. J. Lammers, C. Weenink, U. Yousaf-Khan, N. Horeweg, S. van't Westeinde, M. Prokop, W. P. Mali, F. A. A. M. Hoesein, P. M. A. van Ooijen, J. G. J. V. Aerts, M. A. den Bakker, E. Thunnissen, J. Verschakelen, R. Vliegenthart, J. E. Walter, K. ten Haaf, H. J. M. Groen and M. Oudkerk, *N. Engl. J. Med.*, 2020, **382**, 503–513.
- M. Oudkerk, S. Liu, M. A. Heuvelmans, J. E. Walter and J. K. Field, *Nat. Rev. Clin. Oncol.*, 2021, **18**, 135–151.
- P. Novellis, S. R. Cominesi, F. Rossetti, M. Mondoni, V. Gregorc and G. Veronesi, *Transl. Lung Cancer Res.*, 2021, **10**, 2395–2406.
- C. Liu, X. Xiang, S. Han, H. Y. Lim, L. Li, X. Zhang, Z. Ma, L. Yang, S. Guo, R. Soo, B. Ren, L. Wang and B. C. Goh, *Cancer Lett.*, 2022, **524**, 91–102.
- D. R. Gandara, S. M. Paul, M. Kowanetz, E. Schleifman, W. Zou, Y. Li, A. Rittmeyer, L. Fehrenbacher, G. Otto, C. Malboeuf, D. S. Lieber, D. Lipson, J. Silterra, L. Amler, T. Riehl, C. A. Cummings, P. S. Hegde, A. Sandler, M. Ballinger, D. Fabrizio, T. Mok and D. S. Shames, *Nat. Med.*, 2018, **24**, 1441–1448.
- S. Cai, T. Pataillot-Meakin, A. Shibakawa, R. Ren, C. L. Bevan, S. Ladame, A. P. Ivanov and J. B. Edel, *Nat. Commun.*, 2021, **12**, 3515.
- R. Xing, Y. Wen, Y. Dong, Y. Wang, Q. Zhang and Z. Liu, *Anal. Chem.*, 2019, **91**, 9993–10000.
- L. Ying, L. Du, R. Zou, L. Shi, N. Zhang, J. Jin, C. Xu, F. Zhang, C. Zhu, J. Wu, K. Chen, M. Huang, Y. Wu, Y. Zhang, W. Zheng, X. Pan, B. Chen, A. Lin, J. K. C. Tam, R. M. van Dam, D. T. M. Lai, K. S. Chia, L. Zhou, H.-P. Too, H. Yu, W. Mao and D. Su, *Proc. Natl. Acad. Sci. U. S. A.*, 2020, **117**, 25036–25042.
- J. Zhang, Y. Dong, W. Zhu, D. Xie, Y. Zhao, D. Yang and M. Li, *ACS Appl. Mater. Interfaces*, 2019, **11**, 18145–18152.
- L. Zhao, H. Wang, J. Fu, X. Wu, X. Liang, X. Liu, X. Wu, L. Cao, Z. Xu and M. Dong, *Biosens. Bioelectron.*, 2022, **214**, 114487.
- L. Huang, L. Wang, X. Hu, S. Chen, Y. Tao, H. Su, J. Yang, W. Xu, V. Vedarethinam, S. Wu, B. Liu, X. Wan, J. Lou, Q. Wang and K. Qian, *Nat. Commun.*, 2020, **11**, 3556.
- X. Sun, L. Huang, R. Zhang, W. Xu, J. Huang, D. D. Gurav, V. Vedarethinam, R. Chen, J. Lou, Q. Wang, J. Wan and K. Qian, *ACS Cent. Sci.*, 2018, **4**, 223–229.
- Y. Huang, S. Du, J. Liu, W. Huang, W. Liu, M. Zhang, N. Li, R. Wang, J. Wu, W. Chen, M. Jiang, T. Zhou, J. Cao, J. Yang, L. Huang, A. Gu, J. Niu, Y. Cao, W.-X. Zong, X. Wang, J. Liu, K. Qian and H. Wang, *Proc. Natl. Acad. Sci. U. S. A.*, 2022, **119**, e2122245119.
- H. Zhang, L. Zhao, J. Jiang, J. Zheng, L. Yang, Y. Li, J. Zhou, T. Liu, J. Xu, W. Lou, W. Yang, L. Tan, W. Liu, Y. Yu, M. Ji, Y. Xu, Y. Lu, X. Li, Z. Liu, R. Tian, C. Hu, S. Zhang, Q. Hu, Y. Deng, H. Ying, S. Zhong, X. Zhang, Y. Wang, H. Wang, J. Bai, X. Li and X. Duan, *Nat. Commun.*, 2022, **13**, 617.
- Y. Mu, Y. Zhou, Y. Wang, W. Li, L. Zhou, X. Lu, P. Gao, M. Gao, Y. Zhao, Q. Wang, Y. Wang and G. Xu, *J. Proteome Res.*, 2019, **18**, 2175–2184.
- T. A. Schult, M. J. Lauer, Y. Berker, M. R. Cardoso, L. A. Vandergrift, P. Habbel, J. Nowak, M. Taupitz, M. Aryee, M. A. Mino-Kenudson, D. C. Christiani and L. L. Cheng, *Proc. Natl. Acad. Sci. U. S. A.*, 2021, **118**, e2110633118.
- C. M. Rocha, J. Carrola, A. S. Barros, A. M. Gil, B. J. Goodfellow, I. M. Carreira, J. Bernardo, A. Gomes, V. Sousa, L. Carvalho and I. F. Duarte, *J. Proteome Res.*, 2011, **10**, 4314–4324.
- Y.-J. Chen, T. I. Roumeliotis, Y.-H. Chang, C.-T. Chen, C.-L. Han, M.-H. Lin, H.-W. Chen, G.-C. Chang, Y.-L. Chang, C.-T. Wu, M.-W. Lin, M.-S. Hsieh, Y.-T. Wang, Y.-R. Chen, I. Jonassen, F. Z. Ghavidel, Z.-S. Lin, K.-T. Lin, C.-W. Chen, P.-Y. Sheu, C.-T. Hung, K.-C. Huang, H.-C. Yang, P.-Y. Lin, T.-C. Yen, Y.-W. Lin, J.-H. Wang, L. Raghav, C.-Y. Lin, Y.-S. Chen, P.-S. Wu, C.-T. Lai, S.-H. Weng, K.-Y. Su, W.-H. Chang, P.-Y. Tsai, A. I. Robles, H. Rodriguez, Y.-J. Hsiao, W.-H. Chang, T.-Y. Sung, J.-S. Chen, S.-L. Yu, J. S. Choudhary, H.-Y. Chen, P.-C. Yang and Y.-J. Chen, *Cell*, 2020, **182**, 226–244.
- K. Chen, J. Sun, H. Zhao, R. Jiang, J. Zheng, Z. Li, J. Peng, H. Shen, K. Zhang, J. Zhao, S. Zhu, Y. Wang, F. Yang and J. Wang, *Mol. Cancer*, 2021, **20**, 23.
- S. P. Mulvaney and C. D. Keating, *Anal. Chem.*, 2000, **72**, 145–158.

- 27 B. Lin, Y. Yao, Y. Wang, P. Kannan, L. Chen and L. Guo, *Analyst*, 2021, **146**, 7168–7177.
- 28 Y. Yao, H. Zhang, T. Tian, Y. Liu, R. Zhu, J. Ji and B. Liu, *Talanta*, 2021, **235**, 122728.
- 29 Z. Han, J. Yi, Y. Yang, D. Li, C. Peng, S. Long, X. Peng, Y. Shen, B. Liu and L. Qiao, *Analyst*, 2021, **146**, 6469–6505.
- 30 Y. Yao, J. Ji, H. Zhang, K. Zhang, B. Liu and P. Yang, *Anal. Chem.*, 2018, **90**, 10394–10399.
- 31 T. Tian, J. Yi, Y. Liu, B. Li, Y. Liu, L. Qiao, K. Zhang and B. Liu, *Biosens. Bioelectron.*, 2022, **197**, 113778.
- 32 W. Nam, X. Ren, I. Kim, J. Strobl, M. Agah and W. Zhou, *Anal. Chem.*, 2021, **93**, 4601–4610.
- 33 X. Lin, D. Lin, Y. Chen, J. Lin, S. Weng, J. Song and S. Feng, *Adv. Funct. Mater.*, 2021, **31**, 2103382.
- 34 Y. Zhou, J. Liu, T. Zheng and Y. Tian, *Anal. Chem.*, 2020, **92**, 5910–5920.
- 35 Z. Wang, Y. Hong, H. Yan, H. Luo, Y. Zhang, L. Li, S. Lu, Y. Chen, D. Wang, Y. Su and G. Yin, *Spectrochim. Acta, Part A*, 2022, **279**, 121483.
- 36 J. Lei, D. Yang, R. Li, Z. Dai, C. Zhang, Z. Yu, S. Wu, L. Pang, S. Liang and Y. Zhang, *Spectrochim. Acta, Part A*, 2021, **261**, 120021.
- 37 S. Yang, X. Dai, B. B. Stogin and T.-S. Wong, *Proc. Natl. Acad. Sci. U. S. A.*, 2016, **113**, 268–273.
- 38 S. Kang, I. Kim and P. J. Vikesland, *Anal. Chem.*, 2021, **93**, 9319–9328.
- 39 D. Zhang, H. You, L. Yuan, R. Hao, T. Li and J. Fang, *Anal. Chem.*, 2019, **91**, 4687–4695.
- 40 D. Zhang, L. Peng, X. Shang, W. Zheng, H. You, T. Xu, B. Ma, B. Ren and J. Fang, *Nat. Commun.*, 2020, **11**, 2603.
- 41 Q. Ding, J. Wang, X. Chen, H. Liu, Q. Li, Y. Wang and S. Yang, *Nano Lett.*, 2020, **20**, 7304–7312.
- 42 R. D. Norton, H. T. Phan, S. N. Gibbons and A. J. Haes, *Annu. Rev. Phys. Chem.*, 2022, **73**, 141–162.
- 43 L. Puchades-Carrasco, E. Jantus-Lewintre, C. Pérez-Rambla, F. García-García, R. Lucas, S. Calabuig, A. Blasco, J. Dopazo, C. Camps and A. Pineda-Lucena, *Oncotarget*, 2016, **7**, 12904–12916.
- 44 K. Vanhove, P. Giesen, O. E. Owokotomo, L. Mesotten, E. Louis, Z. Shkedy, M. Thomeer and P. Adriaensens, *BMC Cancer*, 2018, **18**, 868.
- 45 J. Kisluk, M. Ciborowski, M. Niemira, A. Kretowski and J. Niklinski, *J. Pharm. Biomed. Anal.*, 2014, **101**, 40–49.
- 46 L. C. Lee, C. Y. Liong and A. A. Jemain, *Analyst*, 2018, **143**, 3526–3539.
- 47 R. Bujak, E. Dagher-Wojtkowiak, R. Kaliszan and M. J. Markuszewski, *Front. Mol. Biosci.*, 2016, **3**, 35.